Design, Analysis, and Application of Projected k-Winner-Take-All Network

Siqi Liang[1] *Predrag S. Stanimirović*[2] *Bo Peng*[3] *Long Jin*[1*]

[1] *School of Information Science and Engineering, Lanzhou University, Lanzhou, China*
[2] *Faculty of Sciences and Mathematics, Department of Computer Science, University of Niš, Višegradska 33, Niš 18000, Serbia*
[3] *Chongqing Key Laboratory of Big Data and Intelligent Computing, Chongqing Institute of Green and Intelligent Technology, Chinese Academy of Sciences, Chongqing, China*
** E-mail: longjin@ieee.org*

Abstract: Competition is considered to be the driving force of many coordination behaviors, as important as collaboration. To model this competitive nature, an algorithm called k-winner-take-all (kWTA) is introduced that can output k maximum values from input signals. In the process of constructing kWTA network, this paper specially uses a projection function (PF) as the activation function to establish a projected kWTA (P-kWTA) network. Limitations of the activation function selection in traditional models are compensated by employing saturated or even nonconvex PFs in the proposed P-kWTA network. Theoretical analysis proves the global convergence and excellent noise resistance of the P-kWTA network. Besides, the feasibility and effectiveness of the network are demonstrated through numerical simulations and an application on a distributed multi-agent system of competitive coordination.

1 Introduction

Theories such as natural selection and kin selection reveal the fact that competition and collaboration are not contradictory, and they are two different evolutionary paths formed by biological organisms to adapt to the environment. In addition, competition and collaboration are considered to be the internal driving forces of many coordination behaviors in nature [1], such as flying formations, capturing prey, and evading capture. Consensus protocols are often used to model collaborative behaviors and are extensively studied in multi-agent systems [2]. In the biological sense, collaboration refers to the behavior that individuals sacrifice their own fitness to improve the fitness of others, and reciprocal altruism is for better egoism in the future [3]. The environment in which individuals live is equally important for the formation of its behavioral characteristics. In nature, intraspecific competition is more intense than interspecific competition, and the same species struggles cruelly for the same resource demands. Therefore, for coordination behaviors of complex systems, competition and collaboration play an equally important role, and modeling of competitive behaviors is still an open issue.

The operation$k$-winner-take-all (kWTA) can identify the k maximum values from the input signals, which is extensively studied to explore the competitive nature [4]. Maxnet [5] is the first network to implement kWTA, which is a discrete-time network with mutual suppression architecture. A kWTA neural network with a single-layer structure was introduced in [6], which adaptively determines the threshold of each winner through a feedback mechanism rather than inhibition among neurons. The researchers also explore the hardware implementation of kWTA. In [7], the computational power of the WTA circuit is analyzed, which is a variant of kWTA at $k = 1$, and this work proved that the WTA gate could uniquely approximate any continuous function. Moreover, kWTA is generally applied in various fields, especially in multi-agent systems to simulate and capture the nature of competitive behaviors. In [8], a kWTA network with equilibrium points under different input noises (uniform noise and Gaussian noise) was designed and analyzed, and this work also explores how noises affect the network performance. A distributed control method based on competitive coordination was studied in [9] for multi-robot target tracking task under the condition of limited communication with the aid of a consensus protocol. Based on this, a dual-layer kWTA network for finite-time dynamic assignment of multi-agent system was studied for moving target tracking on account of disturbance compensation in [10], where winners perform the task, and the losers return to the origin points. However, the influence of noise perturbation on models is not discussed in the above work. What is more, a robust kWTA network activated by a saturated-allowed function was designed in [11], and it explores a dynamic task assignment problem of multi-agent competitive coordination. This work is the first in realizing the linearization of the kWTA nonlinear system, although it does not explore nonconvex constraints.

The basis of multi-agent coordination is the task assignment, which means that the task to be completed by the whole system must be reasonably distributed among each agent [12]. Given different computing resources and communication environments, there are two types of system architectures for the collaborative task assignment: centralized [8, 10] and distributed [9, 11]. A centralized architecture allows for better distribution by taking global information into account. However, when the autonomous ability of each agent is enhanced, the amount of data that needs to be transmitted increases geometrically due to the dynamic task, which significantly increases the computational complexity and transmission time. Compared to the centralized architecture, the local processing mode of distributed architecture can dramatically reduce the communication load of the entire system with the same amount of computation [13]. For most applications of multi-agent systems, a distributed architecture is preferable to a centralized one, especially when information needs to be obtained remotely [14].

In this paper, a projected kWTA network (P-kWTA) is established, which has global convergence and excellent robustness verified by theoretic analysis. In addition, a distributed multi-agent system synthesized by P-kWTA network is used for the dynamic task assignment based on competitive coordination. The proposed P-kWTA network overcomes the restriction on activation function selection in the traditional models and allows the saturated or even nonconvex projection function (PF). The differences among this paper and other similar works are listed in Table 1.

This work is supported by National Key Research and Development Program of China (No. 2017YFE0118900).

Table 1 Comparisons among this paper and similar works

	Computation Involved	Activation Function	Disturbance Rejection	Steady-state Error	Application	System Architecture
This paper	Yes	Projection Function	Yes	Zero	Multi-agent	Distributed
Paper [4]	Yes	NA	No	Nonzero	Multi-agent	Distributed
Paper [8]	Yes	NA	Yes	Nonzero	Image Processing	Centralized
Paper [9]	Yes	NA	No	Nonzero	Multi-robot	Distributed
Paper [10]	Yes	Adaptive-gain Function	No	Nonzero	Multi-agent	Centralized
Paper [11]	Yes	saturated-allowed Function	Yes	Zero	Multi-agent	Distributed
Paper [15]	No	Projection Function	Yes	Zero	Redundant Robot Manipulators	NA

"NA" means that the detailed information is not mentioned in the corresponding paper.

The rest of this paper is organized into four sections. The transformation of kWTA and the establishment of P-kWTA network are presented in Section 2. Apart from that, theoretical analysis of P-kWTA network is provided in Section 3. In Section 4, numerical simulations of the proposed P-kWTA network and an application of a dynamic tracking task in a multi-agent system are provided. At last, Section 5 is the conclusion of this paper.

2 Problem description and network design

Based on the principle of kWTA and its mathematical characteristics, a P-kWTA network is proposed by adding PFs as activation functions. To make the following process more clear and readable, meaning of the used parameters and symbols are given in Table 2.

Table 2 Parameters definitions in Section 2

$^{\mathrm{T}}$	the transpose of a matrix or a vector
$\circ$	Hadamard product
I	identity matrix
$\mathbf{x}(t)$	the input of kWTA, $\mathbf{x}(t) \in \mathbb{R}^p$
$\mathbf{y}(t)$	the output of kWTA, $\mathbf{y}(t) \in \mathbb{R}^p$
$\mathbf{k}$	the set of the first k maximum in $\mathbf{x}$
$\mathbf{b}(t)$	a coefficient vector, $\mathbf{b}(t) = [1; 1; ...; 1]^{\mathrm{T}} \in \mathbb{R}^{1\times p}$
$B(t)$	a coefficient matrix, $B(t) = 2\gamma I \in \mathbb{R}^{p\times p}$
$\mathbf{a}(t)$	a coefficient vector, $\mathbf{a}(t) = -\mathbf{x}(t) \in \mathbb{R}^p$
$c(t)$	a coefficient, $c(t) = k$
$H(t)$	a coefficient matrix, $H(t) = [I; -I] \in \mathbb{R}^{2p\times p}$
$\mathbf{q}(t)$	a coefficient vector, $\mathbf{q}(t) = [\mathbf{1}_p; \mathbf{0}_p] \in \mathbb{R}^{2p}$
$\lambda(t)$	a Lagrangian multiplier, $\lambda(t) \in \mathbb{R}$
$\boldsymbol{\mu}(t)$	a Lagrangian multiplier, $\boldsymbol{\mu}(t) \in \mathbb{R}^{2p}$

2.1 Problem formulation

According to the introduction above, the kWTA can be described mathematically as

$$\mathbf{y}_i = f(\mathbf{x}_i) = \begin{cases} 1, & \text{if } \mathbf{x}_i \in \mathbf{k} \\ 0, & \text{otherwise,} \end{cases} \tag{1}$$

where $\mathbf{x}$ and $\mathbf{y}$ are the input and output of kWTA, respectively; $\mathbf{x}_i$ and $\mathbf{y}_i$ $(i = 1, 2, \ldots, p)$ are their ith component values, respectively, and $\mathbf{k}$ is a set that contains the first k largest values of $\mathbf{x}$. For better understanding, the operation diagram of kWTA is given in Fig. 1.

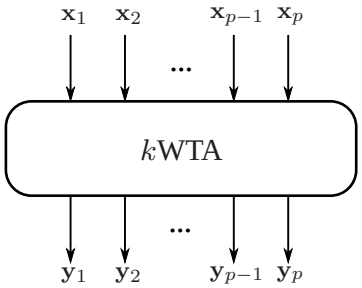

Fig. 1: Schematic diagram of kWTA, where p is the dimension of input $\mathbf{x}$ and output $\mathbf{y}$.

According to [16], kWTA (1) can be equivalently converted into a quadratic programming (QP) problem as

$$\begin{aligned} &\min \gamma \mathbf{y}^{\mathrm{T}}(t)\mathbf{y}(t) - \mathbf{x}^{\mathrm{T}}(t)\mathbf{y}(t) \\ &\text{s. t. } \mathbf{b}(t)\mathbf{y}(t) = k \\ &\quad 0 \le \mathbf{y}_i(t) \le 1, \end{aligned} \tag{2}$$

where γ is a positive constant satisfying $2\gamma < \hat{\mathbf{x}}_k(t) - \hat{\mathbf{x}}_{k+1}(t)$, and $\hat{\mathbf{x}}_i(t)$ represents ith maximum element in $\mathbf{x}(t)$. This constraint guarantees that (2) is a convex problem, and thereby ensures the rationality of using convex optimization theory in later simplified procedures.

Next, the problem (2) is transformed into the following time-varying QP problem with equality and inequality constraints:

$$\begin{aligned} &\min \frac{1}{2}\mathbf{y}^{\mathrm{T}}(t)B(t)\mathbf{y}(t) + \mathbf{a}^{\mathrm{T}}(t)\mathbf{y}(t) \\ &\text{s. t. } \mathbf{b}(t)\mathbf{y}(t) = c(t) \\ &\quad H(t)\mathbf{y}(t) \le \mathbf{q}(t). \end{aligned} \tag{3}$$

In order to find the optimal solution of (3), the corresponding Karush-Kuhn-Tucker (KKT) conditions like [17] are elicited as

$$\begin{cases} B(t)\mathbf{y}(t) + \mathbf{a}(t) + \mathbf{b}^{\mathrm{T}}(t)\lambda(t) + H^{\mathrm{T}}(t)\boldsymbol{\mu}(t) = \mathbf{0} \\ \mathbf{b}(t)\mathbf{y}(t) - c(t) = 0 \\ \boldsymbol{\mu}(t) \ge \mathbf{0},\ \mathbf{q}(t) - H(t)\mathbf{y}(t) \ge \mathbf{0} \\ \boldsymbol{\mu}^{\mathrm{T}}(t)(\mathbf{q}(t) - H(t)\mathbf{y}(t)) = 0, \end{cases} \tag{4}$$

where $\lambda(t)$ is the Lagrangian multiplier of the equality constraint, and $\boldsymbol{\mu}(t)$ is the Lagrangian multiplier corresponding to the inequality constraint. Next, introduce a perturbed Fischer-Burmeister (FB) function [18] as

$$\Phi(\tilde{a}, \tilde{b}) = \tilde{a} + \tilde{b} - \sqrt{\tilde{a} \circ \tilde{a} + \tilde{b} \circ \tilde{b} + \varsigma}. \tag{5}$$

For every $\varsigma \in \mathbb{R}$, it holds $\Phi(\tilde{a}, \tilde{b}) = 0 \Leftrightarrow \tilde{a} > 0, \tilde{b} > 0, \tilde{a}\tilde{b} = 1/2\varsigma$. With the help of characteristics of the FB function, the KKT

conditions (4) can be simplified as

$$\begin{cases} B(t)\mathbf{y}(t)+\mathbf{a}(t)+\mathbf{b}^{\mathrm{T}}(t)\lambda(t)+H^{\mathrm{T}}(t)\boldsymbol{\mu}(t)=\mathbf{0} \\ \mathbf{b}(t)\mathbf{y}(t)-c(t)=0 \\ \Phi(\mathbf{q}(t)-H(t)\mathbf{y}(t),\boldsymbol{\mu}(t))=0. \end{cases} \tag{6}$$

Thus, the above equation can be converted to a nonlinear time-varying equation:

$$E(t)\mathbf{w}(t)-\boldsymbol{\zeta}(t)=\mathbf{0}\in\mathbb{R}^{3p+1}, \tag{7}$$

where $E(t)\in\mathbb{R}^{(3p+1)\times(3p+1)}$ is defined by

$$E(t)=\left[B(t),\mathbf{b}^{\mathrm{T}}(t),H^{\mathrm{T}}(t);\mathbf{b}(t),\mathbf{0},\mathbf{0};-H(t),\mathbf{0},I\right],$$

with $\mathbf{w}(t)=[\mathbf{y}(t);\lambda(t);\boldsymbol{\mu}(t)]\in\mathbb{R}^{3p+1}$,
$\boldsymbol{\zeta}(t)=[-\mathbf{a}(t);c(t);-\mathbf{q}(t)+\boldsymbol{\chi}(t)]\in\mathbb{R}^{3p+1}$,
$\boldsymbol{\chi}(t)=\sqrt{\mathbf{m}(t)\circ\mathbf{m}(t)+\boldsymbol{\mu}(t)\circ\boldsymbol{\mu}(t)+\varsigma}\in\mathbb{R}^{2p}$, and
$\mathbf{m}(t)=\mathbf{q}(t)-H(t)\mathbf{y}(t)\in\mathbb{R}^{2p}$.

2.2 P-kWTA network design

To deal with (7) obtained by kWTA transformation, a vector-valued error function is designed as

$$\boldsymbol{\rho}(t)=E(t)\mathbf{w}(t)-\boldsymbol{\zeta}(t). \tag{8}$$

The design formula corresponding to the error $\boldsymbol{\rho}(t)$ is

$$\dot{\boldsymbol{\rho}}(t)=-\alpha\, G_{\boldsymbol{\upsilon}}(\boldsymbol{\rho}(t)), \tag{9}$$

where $\alpha>0$ is a scaling factor, $G_{\boldsymbol{\upsilon}}(\mathbf{o})$ is an activation function from the set $\mathbf{o}$ to the set $\boldsymbol{\upsilon}$ defined by $G_{\boldsymbol{\upsilon}}(\mathbf{o})=\arg\min_{\mathbf{z}\in\boldsymbol{\upsilon}}\|\mathbf{z}-\boldsymbol{\upsilon}\|_2$, $\mathbf{0}\in\boldsymbol{\upsilon}$ and $\|\cdot\|_2$ is the Euclidean norm. Substituting the error function (8) into the design formula (9) reorganizes

$$E(t)\dot{\mathbf{w}}(t)=-\dot{E}(t)\mathbf{w}(t)+\dot{\boldsymbol{\zeta}}(t)-\alpha G_{\boldsymbol{\upsilon}}(E(t)\mathbf{w}(t)-\boldsymbol{\zeta}(t)).$$

Besides, considering the interference of a noise $\boldsymbol{\sigma}(t)\in\mathbb{R}^{3p+1}$, the proposed P-$k$WTA network is supplied as

$$E(t)\dot{\mathbf{w}}(t)=-\dot{E}(t)\mathbf{w}(t)+\dot{\boldsymbol{\zeta}}(t)-\alpha G_{\boldsymbol{\upsilon}}(E(t)\mathbf{w}(t)-\boldsymbol{\zeta}(t))+\boldsymbol{\sigma}(t). \tag{10}$$

Particularly, some of the PFs offered in this paper are as follows:

- The bound PF:
$\boldsymbol{\upsilon}=\{\mathbf{o}\in\mathbb{R}^{3p+1},\ \check{\mathcal{R}}\le\mathbf{o}_i\le\hat{\mathcal{R}}\ \text{or}\ \mathbf{o}_i=\check{\mathcal{R}}\ \text{or}\ \mathbf{o}_i=\hat{\mathcal{R}}\}$ where $\check{\mathcal{R}}<0<\hat{\mathcal{R}}$.
- The powersum PF: $G_{\boldsymbol{\upsilon}}(\mathbf{o})=\mathbf{o}+\mathbf{o}^3+\mathbf{o}^5$.
- The powersigmoid PF:

$$G_{\boldsymbol{\upsilon}}(\mathbf{o}_i)=\begin{cases}\mathbf{o}_i^2, & |\mathbf{o}_i|\ge 1\\ \frac{1+\exp(-4)}{1-\exp(-4)}\times\frac{1-\exp(-4\mathbf{o}_i)}{1+\exp(-4\mathbf{o}_i)}, & |\mathbf{o}_i|<1.\end{cases}$$

- The nonconvex PF:
$\boldsymbol{\upsilon}=\{\mathbf{o}\in\mathbb{R}^{3p+1},\ -\varsigma_1\le\mathbf{o}_i\le\varsigma_1\ \text{or}\ \mathbf{o}_i=\varsigma_2\ \text{or}\ \mathbf{o}_i=\varsigma_3\}$ where the constant terms $\varsigma_1,\varsigma_2,\varsigma_3$ satisfy $0<\varsigma_1<\varsigma_2$ and $\varsigma_3<-\varsigma_1<0$.

3 Theoretical analysis

The following theoretical results demonstrate the convergence and robustness of the proposed P-kWTA network (10).

Theorem 1: The residual error $\boldsymbol{\rho}(t)$ of the P-kWTA network (10) without noise perturbation achieves global convergence to zero.

Proof: A Lyapunov candidate function is defined as

$$\chi(t)=\boldsymbol{\rho}^{\mathrm{T}}(t)\boldsymbol{\rho}(t)/2. \tag{11}$$

Thus, one can acquire that if $\boldsymbol{\rho}(t)\neq 0$, it has $\chi(t)>0$; otherwise, if $\boldsymbol{\rho}(t)=0$, there must be $\chi(t)=0$, which explains the positive definiteness of (11). Furthermore, taking time derivative of the above equation gets

$$\dot{\chi}(t)=\boldsymbol{\rho}^{\mathrm{T}}(t)\dot{\boldsymbol{\rho}}(t).$$

Combining the above equation with (9) elicits

$$\dot{\chi}(t)=-\alpha G_{\boldsymbol{\upsilon}}^{\mathrm{T}}(\boldsymbol{\rho}(t))\boldsymbol{\rho}(t). \tag{12}$$

According to the definition of $G_{\boldsymbol{\upsilon}}(\cdot)$, one can obtain

$$\|\mathbf{z}-\boldsymbol{\rho}(t)\|_2^2\ge\|G_{\boldsymbol{\upsilon}}(\boldsymbol{\rho}(t))-\boldsymbol{\rho}(t)\|_2^2,\ \forall\mathbf{z}\in\boldsymbol{\upsilon}. \tag{13}$$

For $\mathbf{z}=\mathbf{0}$, a conclusion can be drawn as

$$\|\boldsymbol{\rho}(t)\|_2^2\ge\|G_{\boldsymbol{\upsilon}}(\boldsymbol{\rho}(t))-\boldsymbol{\rho}(t)\|_2^2.$$

An expansion of the above formula further leads to

$$0\le G_{\boldsymbol{\upsilon}}^{\mathrm{T}}(\boldsymbol{\rho}(t))G_{\boldsymbol{\upsilon}}(\boldsymbol{\rho}(t))\le 2G_{\boldsymbol{\upsilon}}^{\mathrm{T}}(\boldsymbol{\rho}(t))\boldsymbol{\rho}(t).$$

Combining the above equation and (12) gains

$$\dot{\chi}(t)\le-G_{\boldsymbol{\upsilon}}^{\mathrm{T}}(\boldsymbol{\rho}(t))G_{\boldsymbol{\upsilon}}(\boldsymbol{\rho}(t))/2\le 0. \tag{14}$$

Hence, on the basis of Lyapunov theory [19], it is concluded that the residual error $\boldsymbol{\rho}(t)$ of the proposed P-kWTA network (10) globally converges to zero in the noise-free situation. ■

Theorem 2: Let the PF choose a bound in which $\hat{\mathcal{R}}$ and $\check{\mathcal{R}}$ are the upper and lower bounds, respectively. Assuming that a noise satisfying $\alpha\check{\mathcal{R}}\prec\boldsymbol{\sigma}(t)\prec 0$ or $0\prec\boldsymbol{\sigma}(t)\prec\alpha\hat{\mathcal{R}}$ is injected, the residual error $\boldsymbol{\rho}(t)$ of the proposed P-kWTA network (10) achieves a global convergence to a constant value $G_{\boldsymbol{\upsilon}}^{-1}(\boldsymbol{\sigma}(t)/\alpha)$.

Proof: Perturbed by the input noise $\boldsymbol{\sigma}(t)$, the ith subsystem of (9) is written as

$$\dot{\boldsymbol{\rho}}_i(t)=-\alpha G_{\boldsymbol{\upsilon}_i}(\boldsymbol{\rho}_i(t))+\boldsymbol{\sigma}_i(t), \tag{15}$$

where $G_{\boldsymbol{\upsilon}}(\cdot)$ denotes an array of the bound PFs. Next, construct a Lyapunov candidate function as

$$\nu_i(t)=\boldsymbol{\rho}_i^2(t)/2. \tag{16}$$

Analogous as in the proof in Theorem 1, it is concluded that (16) is non-negative. Then, taking time derivative of the above equation and combining it with (15) gives

$$\dot{\nu}_i(t)=\boldsymbol{\rho}_i(t)(-\alpha G_{\boldsymbol{\upsilon}_i}(\boldsymbol{\rho}_i(t))+\boldsymbol{\sigma}_i(t)). \tag{17}$$

Since the evolution of $\dot{\nu}_i(t)$ changes over time, the analysis of (17) has the following cases: 1) $\boldsymbol{\rho}_i(t)<0$; 2) $\boldsymbol{\rho}_i(t)>0$; 3) $\boldsymbol{\rho}_i(t)=0$.

1) For the case $\boldsymbol{\rho}_i(t)<0$, there are the following three subcases:
   i) For the subcase $-\alpha G_{\boldsymbol{\upsilon}_i}(\boldsymbol{\rho}_i(t))+\boldsymbol{\sigma}_i(t)>0$, it can be derived that $\dot{\nu}_i(t)<0$, which assures globally convergence of $\boldsymbol{\rho}_i(t)$, and then $G_{\boldsymbol{\upsilon}_i}(\boldsymbol{\rho}_i(t))$ increases until $\boldsymbol{\rho}_i(t)=G_{\boldsymbol{\upsilon}_i}^{-1}(\boldsymbol{\sigma}_i(t)/\alpha)$. In this subcase, $\boldsymbol{\rho}_i(t)$ converges along the curve f in Fig. 2.
   ii) For the subcase $-\alpha G_{\boldsymbol{\upsilon}_i}(\boldsymbol{\rho}_i(t))+\boldsymbol{\sigma}_i(t)=0$, it can be deduced $\dot{\nu}_i(t)=0$, and then $\boldsymbol{\rho}_i(t)=G_{\boldsymbol{\upsilon}_i}^{-1}(\boldsymbol{\sigma}_i(t)/\alpha)$, which reflects that subsystem (15) is currently in a stable state. In this subcase, $\boldsymbol{\rho}_i(t)$ remains on the fixed line b described in Fig. 2.

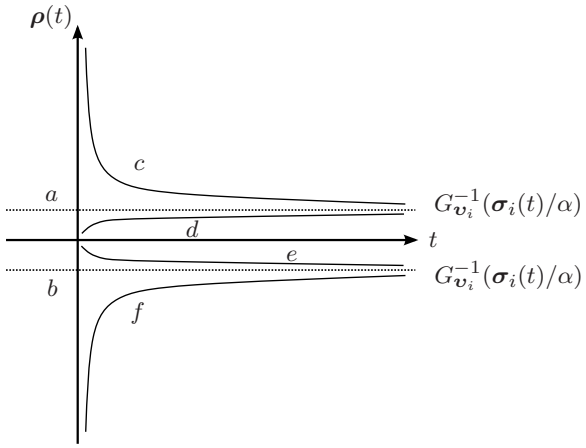

Fig. 2: Convergence process of residual error $\boldsymbol{\rho}(t)$.

iii) For the subcase $-\alpha G_{\boldsymbol{\upsilon}_i}(\boldsymbol{\rho}_i(t)) + \boldsymbol{\sigma}_i(t) < 0$, it can be deduced $\dot{\nu}_i(t) > 0$, which means that the subsystem (15) is diverging at present, and thereby $|\boldsymbol{\rho}_i(t)|$ and $|G_{\boldsymbol{\upsilon}_i}(\boldsymbol{\rho}_i(t))|$ increase with time changing correspondingly. However, since PF is chosen as a bounded function that has a lower bound $\check{\mathcal{R}}_i$, the following two discussions are generated.
a) $\alpha\check{\mathcal{R}}_i \leq \boldsymbol{\sigma}_i(t)$: The residual error is still constrained by $G_{\boldsymbol{\upsilon}_i}^{-1}(\boldsymbol{\sigma}_i(t)/\alpha)$, and then subsystem (15) inevitably reverts to subcase ii) and becomes stable. In this sense, the subsystem diverges with a bound $\boldsymbol{\rho}_i(t) = G_{\boldsymbol{\upsilon}_i}^{-1}(\boldsymbol{\sigma}_i(t)/\alpha)$ along the curve e portrayed in Fig. 2.
b) $\alpha\check{\mathcal{R}}_i > \boldsymbol{\sigma}_i(t)$: Then, α needs to be adjusted larger to get the subsystem (15) out of divergence.

2) For the case $\boldsymbol{\rho}_i(t) > 0$, there are the following three cases:
i) If $-\alpha G_{\boldsymbol{\upsilon}_i}(\boldsymbol{\rho}_i(t)) + \boldsymbol{\sigma}_i(t) < 0$, it is concluded that $\dot{\nu}_i(t) < 0$, which assures that $\boldsymbol{\rho}_i(t)$ is globally convergent, and then $G_{\boldsymbol{\upsilon}_i}(\boldsymbol{\rho}_i(t))$ decreases as time until $\boldsymbol{\rho}_i(t) = G_{\boldsymbol{\upsilon}_i}^{-1}(\boldsymbol{\sigma}_i(t)/\alpha)$. In this subcase, $\boldsymbol{\rho}_i(t)$ converges along the curve c in Fig. 2.
ii) If $-\alpha G_{\boldsymbol{\upsilon}_i}(\boldsymbol{\rho}_i(t)) + \boldsymbol{\sigma}_i(t) = 0$, it can be deduced $\dot{\nu}_i(t) = 0$, and then $\boldsymbol{\rho}_i(t) = G_{\boldsymbol{\upsilon}_i}^{-1}(\boldsymbol{\sigma}_i(t)/\alpha)$, which reflects that subsystem (15) is currently in a stable state. In this subcase, $\boldsymbol{\rho}_i(t)$ remains on the fixed line a depicted in Fig. 2.
iii) If $-\alpha G_{\boldsymbol{\upsilon}_i}(\boldsymbol{\rho}_i(t)) + \boldsymbol{\sigma}_i(t) > 0$, it is concluded that $\dot{\nu}_i(t) > 0$, which means that the subsystem (15) is diverging at present. Similar to the discussion in 1), since PF is chosen as a bound function which has an upper bound $\hat{\mathcal{R}}_i$, the following two discussions are generated.
a) $\alpha\hat{\mathcal{R}}_i \geq \boldsymbol{\sigma}_i(t)$: The residual error is still constrained by $G_{\boldsymbol{\upsilon}_i}^{-1}(\boldsymbol{\sigma}_i(t)/\alpha)$. Similarly, the subsystem (15) inevitably reverts to subcase ii) and becomes stable. In this sense, the subsystem diverges with a bound $\boldsymbol{\rho}_i(t) = G_{\boldsymbol{\upsilon}_i}^{-1}(\boldsymbol{\sigma}_i(t)/\alpha)$ along the curve d portrayed in Fig. 2.
b) $\alpha\hat{\mathcal{R}}_i < \boldsymbol{\sigma}_i(t)$: Then, α needs to be adjusted larger to get the subsystem (15) out of divergence.

3) For the case $\boldsymbol{\rho}_i(t) = 0$, it is concluded that $G_{\boldsymbol{\upsilon}_i}(\boldsymbol{\rho}_i(t)) = 0$, and then $\dot{\boldsymbol{\rho}}_i(t) = \boldsymbol{\sigma}_i(t)$. By this time, $\boldsymbol{\rho}_i(t)$ is in a state of instantaneous change, and the subsystem (15) is unstable, and thereby the discussion goes back to case 1) $\boldsymbol{\rho}_i(t) < 0$ or 2) $\boldsymbol{\rho}_i(t) > 0$.

A summary of the above discussion is that, when supposing $\alpha\check{\mathcal{R}} \prec \boldsymbol{\sigma}(t) \prec 0$ or $0 \prec \boldsymbol{\sigma}(t) \prec \alpha\hat{\mathcal{R}}$, there is $\lim_{t\to\infty} \boldsymbol{\rho}(t) = G_{\boldsymbol{\upsilon}}^{-1}(\boldsymbol{\sigma}(t)/\alpha)$, where $G_{\boldsymbol{\upsilon}}^{-1}(\boldsymbol{\sigma}(t)/\alpha)$ represents a constant value. This means that the residual error of the proposed P-kWTA network (10) is of global convergence toward the fixed value $G_{\boldsymbol{\upsilon}}^{-1}(\boldsymbol{\sigma}(t)/\alpha)$ with the unknown noise $\boldsymbol{\sigma}(t)$ injected. Namely, when $\alpha \geq \max\left\{\max\{|\boldsymbol{\sigma}_i(t)|/|\check{\mathcal{R}}_i|\}, \max\{\boldsymbol{\sigma}_i(t)/\hat{\mathcal{R}}_i\}\right\}$, $\boldsymbol{\rho}(t)$ is always globally convergent. ■

Theorem 3: When the PF is unbounded and a constant noise $\boldsymbol{\sigma}(t)$ is injected, the residual error $\boldsymbol{\rho}(t)$ of the proposed P-kWTA network (10) accomplishes global convergence to a constant value $G_{\boldsymbol{\upsilon}}^{-1}(\boldsymbol{\sigma}(t)/\alpha)$.

Proof: With an unbounded PF aided, the ith subsystem of (9) is written as

$$\dot{\boldsymbol{\rho}}_i(t) = -\alpha\, G_{\boldsymbol{\upsilon}_i}(\boldsymbol{\rho}_i(t)) + \boldsymbol{\sigma}_i(t), \tag{18}$$

where $G_{\boldsymbol{\upsilon}}(\cdot)$ represents an array of an unbounded PF. Moreover, a Lyapunov candidate function is defined as

$$\nu_i(t) = \boldsymbol{\rho}_i^2(t)/2. \tag{19}$$

Equally, a conclusion is that $\nu_i(t)$ is positive definite. Then, taking the time derivative of the above equation and combining it with (18), it can be obtained

$$\dot{\nu}_i(t) = \boldsymbol{\rho}_i(t)(-\alpha G_{\boldsymbol{\upsilon}_i}(\boldsymbol{\rho}_i(t)) + \boldsymbol{\sigma}_i(t)). \tag{20}$$

Since the evolution of $\dot{\nu}_i(t)$ changes over time, the analysis of (20) can be divided into the following two phases: 1) $\boldsymbol{\rho}_i(t) \neq 0$; 2) $\boldsymbol{\rho}_i(t) = 0$.

1) For the case $\boldsymbol{\rho}_i(t) \neq 0$, i.e., $\boldsymbol{\rho}_i(t) > 0$ or $\boldsymbol{\rho}_i(t) < 0$, in which one deduces that $G_{\boldsymbol{\upsilon}_i}(\boldsymbol{\rho}_i(t)) \neq 0$. To further verify $\dot{\nu}_i(t) < 0$, the following two subcases are considered:
i) For the subcase $-\alpha G_{\boldsymbol{\upsilon}_i}(\boldsymbol{\rho}_i(t)) + \boldsymbol{\sigma}_i(t) \neq 0$. There must be a time to make $-\alpha G_{\boldsymbol{\upsilon}_i}(\boldsymbol{\rho}_i(t)) + \boldsymbol{\sigma}_i(t) > 0$ for $\boldsymbol{\rho}_i(t) < 0$ or $-\alpha G_{\boldsymbol{\upsilon}_i}(\boldsymbol{\rho}_i(t)) + \boldsymbol{\sigma}_i(t) < 0$ for $\boldsymbol{\rho}_i(t) > 0$. Simultaneously, it is deduced $\dot{\nu}_i(t) < 0$, and then $\boldsymbol{\rho}_i(t)$ converges globally. In this situation, the residual error $\boldsymbol{\rho}_i(t)$ converges along the curves c, d, e, or f as exhibited in Fig. 2.
ii) The subcase $-\alpha G_{\boldsymbol{\upsilon}_i}(\boldsymbol{\rho}_i(t)) + \boldsymbol{\sigma}_i(t) = 0$ determines $\dot{\nu}_i(t) = 0$, and then $\boldsymbol{\rho}_i(t) = G_{\boldsymbol{\upsilon}_i}^{-1}(\boldsymbol{\sigma}_i(t)/\alpha)$, which reflects that subsystem (18) is currently in a stable state and $\boldsymbol{\rho}_i(t)$ stays at the fixed lines a or b in Fig. 2.

2) For the case $\boldsymbol{\rho}_i(t) = 0$, there must be $G_{\boldsymbol{\upsilon}_i}(\boldsymbol{\rho}_i(t)) = 0$. In this situation, it must has $\dot{\boldsymbol{\rho}}_i(t) = \boldsymbol{\sigma}_i(t)$. Similarly, $\dot{\boldsymbol{\rho}}_i(t) > 0$ for $\boldsymbol{\sigma}_i(t) > 0$ and $\dot{\boldsymbol{\rho}}_i(t) < 0$ for $\boldsymbol{\sigma}_i(t) < 0$. At this time, $\boldsymbol{\rho}_i(t) = 0$ is only an instantaneous state and subsystem (18) is unstable. Then the discussion returns to the case 1).

In summary, when the constant noise $\boldsymbol{\sigma}(t)$ is injected, and the PF is an unbounded function, the residual error of the proposed P-kWTA network (10) could reach a global convergence to a constant value $G_{\boldsymbol{\upsilon}}^{-1}(\boldsymbol{\sigma}(t)/\alpha)$. ■

Theorem 4: When the PF selects a linear one and a bound noise $\boldsymbol{\sigma}(t)$ is injected, the residual error $\boldsymbol{\rho}(t)$ of the proposed P-kWTA network (10) is bounded with $\lim_{t\to\infty} \sup \|\boldsymbol{\rho}(t)\|_2 \leq q\sqrt{3p+1}/\alpha$, where $q = \max_{1\leq i\leq 3p+1}\{\max_{0\leq o\leq t} |\boldsymbol{\sigma}_i(o)|\}$.

Proof: Under the linear PF, the ith subsystem of (9) polluted by a bounded noise could be composed as

$$\dot{\boldsymbol{\rho}}_i(t) = -\alpha\, G_{\boldsymbol{\upsilon}_i}(\boldsymbol{\rho}_i(t)) + \boldsymbol{\sigma}_i(t),\ \forall i \in 1, \ldots, 3p, 3p+1, \tag{21}$$

where $\alpha\, G_{\boldsymbol{\upsilon}}(\cdot)$ denotes an array of the linear PF, and $\boldsymbol{\sigma}_i(t)$ represents the bounded noise. Then the solution of the above equation is elicited as

$$\boldsymbol{\rho}_i(t) = \boldsymbol{\rho}_i(0)e^{-\alpha t} + \int_0^t e^{-\alpha(t-o)}\boldsymbol{\sigma}_i(o)\mathrm{d}o.$$

According to the principle of triangle inequality, the above equation can be further transformed into

$$\begin{aligned} |\boldsymbol{\rho}_i(t)| &\leq |\boldsymbol{\rho}_i(0)e^{-\alpha t}| + \left|\int_0^t e^{-\alpha(t-o)}\boldsymbol{\sigma}_i(o)\mathrm{d}o\right| \\ &\leq |\boldsymbol{\rho}_i(0)e^{-\alpha t}| + \int_0^t \left|e^{-\alpha(t-o)}\right| |\boldsymbol{\sigma}_i(o)|\,\mathrm{d}o. \end{aligned}$$

To further simplify the above formula, one obtains

$$|\boldsymbol{\rho}_i(t)| \leq |\boldsymbol{\rho}_i(0)e^{-\alpha t}| + \frac{1}{\alpha}\max_{0\leq o\leq t} |\boldsymbol{\sigma}_i(o)|.$$

Furthermore, a conclusion can be drawn as

$$\lim_{t\to\infty}\sup\|\boldsymbol{\rho}(t)\|_2 \leq \frac{q\sqrt{3p+1}}{\alpha}, \tag{22}$$

where q denotes $\max_{1\leq i\leq 3p+1}\{\max_{0\leq o\leq t}|\boldsymbol{\sigma}_i(o)|\}$. What is more, it is derived that $\lim_{t\to\infty}\|\boldsymbol{\rho}(t)\|_2$ is inversely proportional to α. ■

4 Illustrative examples

In this section, numerical simulations of the proposed P-kWTA network (10) with different PFs are offered and analyzed. In addition, a distributed P-kWTA system synthesized by the P-kWTA network (10) is applied to multi-agent dynamic task assignment based on competitive coordination.

4.1 Numerical simulations

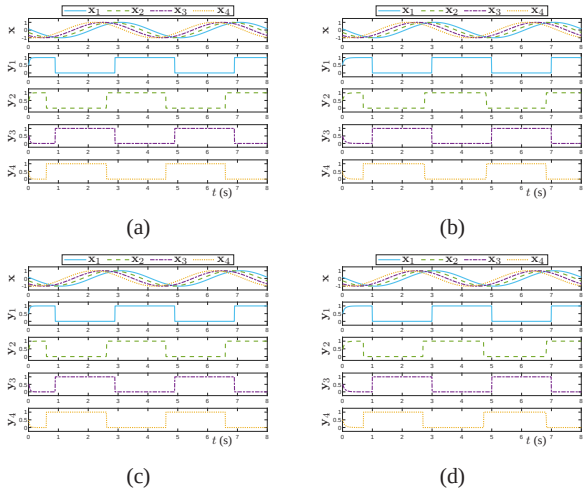

Fig. 3: Numerical results generated by the proposed P-kWTA network (10) with different PFs. (a) Bound PF. (b) Powersum PF. (c) Powersigmoid PF. (d) Nonconvex PF.

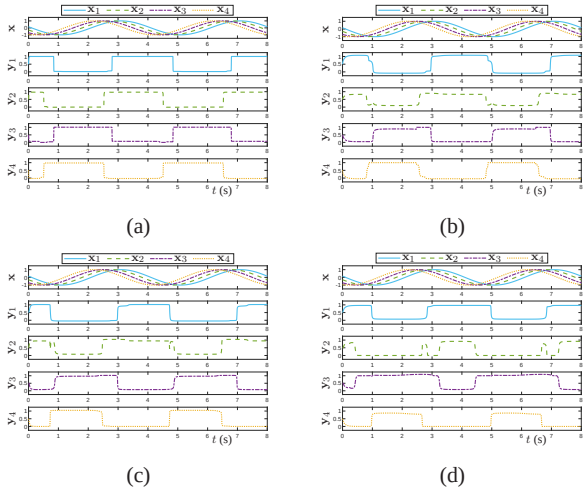

Fig. 4: Numerical results generated by the proposed P-kWTA network (10) with different PFs with constant noise perturbation. (a) Bound PF. (b) Powersum PF. (c) Powersigmoid PF. (d) Nonconvex PF.

In order to verify the validity and robustness of the proposed P-kWTA network (10), one considers a set of four cosine input data $\mathbf{x}_i = \cos(0.5\pi(t+0.9+0.3(i-1)))$, $(i=1,2,3,4)$, and thereby $p=4$; the number of winners is $k=2$; design parameter $\alpha=10$; execution time $T=8$s. Moreover, define constant noise set within $[-3,3]$. Time-dependent behaviors corresponding to input $\mathbf{x}_i$ and output $\mathbf{y}_i$ with four different PFs (bound, powersum, powersigmoid, and nonconvex) without perturbations are displayed in Fig. 3, and simulations with noise interference is depicted in Fig. 4. What is more, figures in this paper are all represented by normalized units. It is manifested from Fig. 3 that the status outputs always ensure two zeros and two ones at the same time, which means that the proposed P-kWTA network (10) is able to select the k maximums from the time-dependent inputs precisely. As plotted in Fig. 4, the network (10) can also perform tasks accurately with noise injection, which summarizes that each PF ensures different noise resistance. It is worth noting that different PFs are used to accelerate the convergence of the proposed P-kWTA network (10), and thus the other PFs simulations are omitted.

4.2 Simulation examples

Consider p agents in 3-D space jointly tracking one target, of which k agents can win out and be selected to perform the tracking task, and the rest ones remain stationary in the current position. Then, the input of kWTA (1) is designed as

$$\mathbf{x}_i = -\|\varrho_i - \varrho_{\mathrm{o}}\|_2^2/2, \tag{23}$$

where ϱ_i and ϱ_{o} represent the ith agent's position and the chasing target position, respectively. The speed of each agent is set as $\dot{\varrho}_i = \mathbb{e}\mathbf{y}_i\partial\mathbf{x}_i/\partial\varrho_i$, and $\mathbb{e}>0$ is a parameter related to the rate of convergence, with $\mathbb{e}=10$ here; the target speed is set as $v_{\mathrm{o}} = -7\exp(-t)\varrho_{\mathrm{o}}/\|\varrho_{\mathrm{o}}\|$. The agent group communication rule is organized so that agents can send information with each other if the distance is less than the critical distance. Otherwise, they cannot send information. Therefore, its communication topology is not necessarily a fully connected graph. Furthermore, it can be known from the transformation from (1) to (7) that $E(t)$ is a time invariant matrix, so the dynamic characteristics of the network are guaranteed by the time-varying input $\mathbf{x}(t)$. However, in the process of exploiting the P-kWTA network (10), a condition $\sum_{i=1}^{p}\mathbf{y}_i(t)=k$ must be satisfied, which means that all agents' states are indispensable in network computing. Based on this, a consensus estimator presented in [20] is

Algorithm 1 Competitive coordination of multi-agent system

Input: Number of agents and winners p and k, respectively, noise $\boldsymbol{\sigma}(t)$, critical distance d_f for task completion;
Output: Tracking trajectory;
1: Random initialization $\varrho_{\mathrm{o}}(\varrho_{\mathrm{o}_x},\varrho_{\mathrm{o}_y},\varrho_{\mathrm{o}_z})$, $\varrho_i(\varrho_{i_x},\varrho_{i_y},\varrho_{i_z})$, $\forall i=1,...,p$;
2: Initialize $\mathbf{x}(0)=\mathbf{0}_p$, $\mathbf{y}(0)=\mathbf{0}_p$, $\boldsymbol{\zeta}(0)=[\mathbf{x}(0);k;-\mathbf{q}(0)+\boldsymbol{\chi}(0)]$, $E(t)=[2\gamma I,\mathbf{1}_p,[I;-I]^{\mathrm{T}};\mathbf{1}_p^{\mathrm{T}},0,\mathbf{0}_{2p}^{\mathrm{T}};-[I;-I],\mathbf{0}_{2p},I]$;
3: **repeat**
4: Control target movement according to v_{o};
5: Calculate $\mathbf{x}_i=-\|\varrho_i-\varrho_{\mathrm{o}}\|_2^2/2$, $\forall i=1,...,p$;
6: Update $\boldsymbol{\zeta}(t)=[\mathbf{x}(t);k;-\mathbf{q}(t)+\boldsymbol{\chi}(t)]$;
7: Calculate $\mathbf{w}(t)$ according to $\dot{\mathbf{w}}=E^{-1}(-\dot{E}\mathbf{w}(t)+\dot{\boldsymbol{\zeta}}(t)-\alpha G_{\boldsymbol{\upsilon}}(E\mathbf{w}(t)-\boldsymbol{\zeta}(t))+\boldsymbol{\sigma}(t))$;
8: Calculate $\dot{\varrho}_i=\mathbb{e}\mathbf{y}_i\partial\mathbf{x}_i/\partial\varrho_i$, $\forall i=1,...,p$;
9: Control agent movement according to $\dot{\varrho}_i$;
10: **until** $\|\mathbf{y}_i(\varrho_i-\varrho_{\mathrm{o}})\|_2<d_f$;

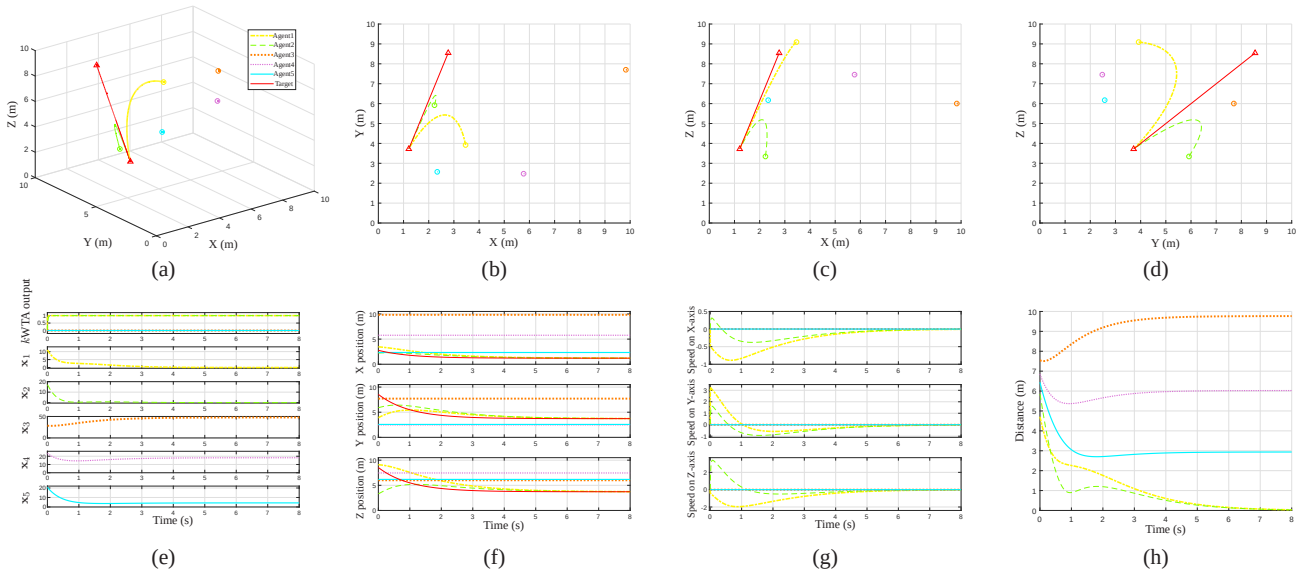

Fig. 5: Simulation results synthesized by the distributed P-kWTA system (25) with $n = 5$ and $k = 2$ without perturbation and activated by the bound PF. (a) Movement trajectory in 3-D space. (b) Trajectory on the $X-Y$ plane. (c) Trajectory on the $X-Z$ plane. (d) Trajectory on the $Y-Z$ plane. (e) Input and output of kWTA. (f) Position of agents. (g) Speed of agents. (h) Linear distance between agents and the target.

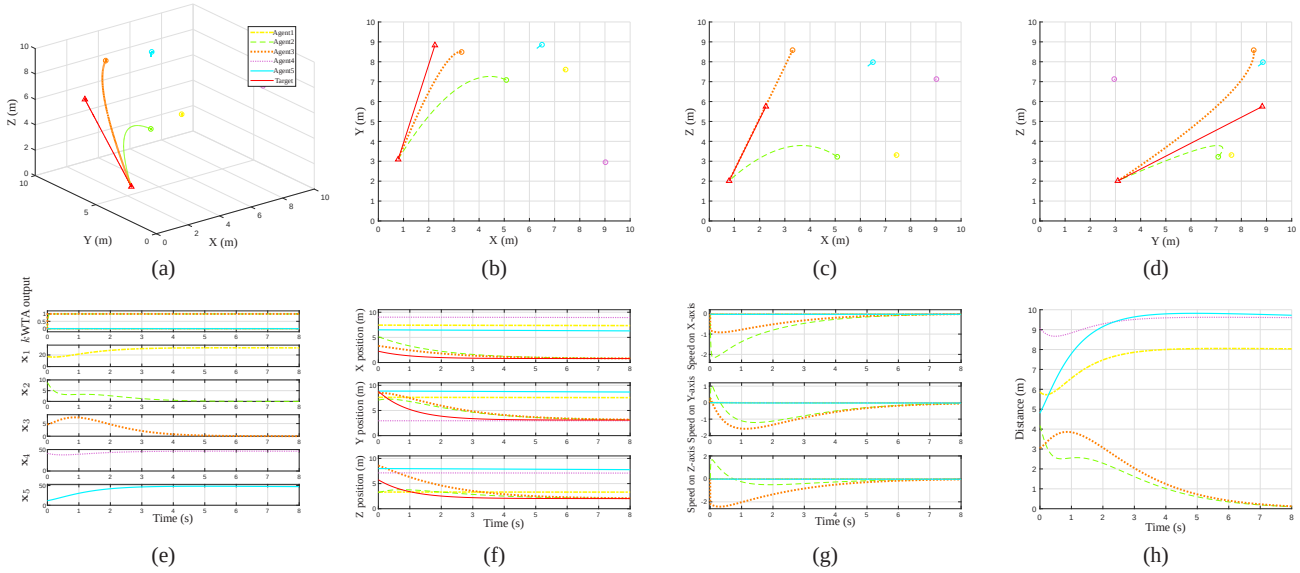

Fig. 6: Simulation results synthesized by the distributed P-kWTA system (25) with $n = 5$ and $k = 2$ with random noise and activated by the bound PF. (a) Movement trajectory in 3-D space. (b) Trajectory on the $X-Y$ plane. (c) Trajectory on the $X-Z$ plane. (d) Trajectory on the $Y-Z$ plane. (e) Input and output of kWTA. (f) Position of agents. (g) Speed of agents. (h) Linear distance between agents and the target.

introduced here to estimate the average of kWTA (1) outputs:

$$\begin{aligned}\dot{d}_i &= -\mu\left[\sum_{j\in\mathcal{N}_i}\mathcal{Q}_{ij}(d_i-d_j)+\sum_{j\in\mathcal{N}_i}\mathcal{Q}_{ij}(f_i-f_j)+(d_i-\mathbf{y}_i)\right],\\ \dot{f}_i &= \sum_{j\in\mathcal{N}_i}\mathcal{Q}_{ij}(d_i-d_j),\end{aligned} \tag{24}$$

where d_i is an estimation of $\sum_{i=1}^{p}\mathbf{y}_i(t)/p$; $\mu>0$ is a scaling parameter and $\mu=10$ is chosen; $\mathcal{N}_i$ is a set of ith agent's neighbors in the communication topology; $\mathcal{Q}$ is the adjacency matrix of the communication topology, and $\mathcal{Q}_{ij}$ implies the element in row i, column j; f_i is a scalar state for ith agent. Next, combining the above equations with (10), a distributed P-kWTA system for the dynamic tracking task of multi-agent system is organized as follows:

$$\begin{aligned}\dot{\varrho}_i &= \Phi\mathbf{y}_i\partial\mathbf{x}_i/\partial\varrho_i,\\ \mathbf{y}_i &= \mathbf{w}(1:p),\\ \dot{\mathbf{w}} &= E^{-1}(-\dot{E}\mathbf{w}(t)+\dot{\boldsymbol{\zeta}}(t)-\alpha G_{\boldsymbol{\upsilon}}(E\mathbf{w}(t)-\boldsymbol{\zeta}(t))+\boldsymbol{\sigma}(t)),\\ \dot{d}_i &= -\mu\left[\sum_{j\in\mathcal{N}_i}\mathcal{Q}_{ij}(d_i-d_j)+\sum_{j\in\mathcal{N}_i}\mathcal{Q}_{ij}(f_i-f_j)+(d_i-\mathbf{y}_i)\right],\\ \dot{f}_i &= \sum_{j\in\mathcal{N}_i}\mathcal{Q}_{ij}(d_i-d_j).\end{aligned} \tag{25}$$

Moreover, the detailed steps are given as Algorithm 1.

Next, all parameters involved in the distributed P-kWTA system (25) are defined as agents number $p = 5$; winners number $k = 2$; design parameter $\alpha = 10$; execution time $T = 8$s; random noise range $\boldsymbol{\sigma}(t) \in [0, 0.5]^{16}$. The initial positions of agents and target are optionally placed within the range of $[-10, 10]$ m on X, Y, and Z-axes.

In order to observe the effect of system (25) applied in multi-agent coordination, Figs. 5-6 respectively exhibit the tracking trajectory with and without noise perturbation, the output of kWTA, the position and speed changes of agents on the X, Y, and Z axes, and the linear distance from the target. In this sense, five agents participate in the competition, and only two winning agents are selected to further track the specified target, while the rest of losers are not driven. Furthermore, Figs. 5(a) and 6(a) portray initial positions of the target and agents as well as the tracking trajectory. In order to demonstrate the tracking process more explicitly, Figs. 5(b)-(d) and 6(b)-(d) are trajectories of the projection on the $X-Y$, $X-Z$, and $Y-Z$ planes. The input $\mathbf{x}_i$ for each agent and output $\mathbf{y}$ of kWTA are illustrated in Figs. 5(e) and 6(e). According to the definition of $\mathbf{x}_i$, it can be aware of that the system (25) can effectively assign tasks to the two optimal agents. Besides, Figs. 5(f) and 6(f) plot movement positions of the target and agents in three directions. It is observed that the target is finally captured by agents 1 and 2 without noise, and agents 2 and 3 are winners with noise. This result can also be verified in Figs. 5(g) and 6(g), which illustrate the speed component of agents on three axes X, Y, and Z. It serves to show that with the completion of the tracking task, speeds of the winning agents gradually drop to zero. The variation of linear distances between agents and the target over time is plotted in Figs. 5(h) and 6(h), and only the winners' distances finally drop to zero. That is, the task is completed successfully. Noting that the noise injection may cause confusion in the tracking task at the initial stage, but the network can quickly correct the error. For example, the blue trajectory in Fig. 6(a)-(d) means that the agent 5 moves in the early stage, but its position and velocity curves in Fig. 6(f) and (g) both express that this agent does not move.

In short, numerical and computer simulations both demonstrate the efficiency and robustness of the P-kWTA network (10) and the distributed P-kWTA system (25) for competitive coordination among agents.

5 Conclusion

In this paper, in order to explore the dynamic task assignment problem in multi-agent coordination, a P-kWTA network using PFs as activation function has been explored and used in target tracking task. Theoretical analyses have demonstrated that the P-kWTA network possesses global convergence and excellent robustness against noise. Finally, through simulations, the superiority, effectiveness, and accuracy of the distributed P-kWTA system synthesized by P-kWTA network for multi-agent competitive coordination tasks in noisy and noise-free environments have been verified.

6 References

1 Axelrod, R., Hamilton, W.D.: 'The evolution of cooperation', *Science*, 1981, **211**, (4489), pp. 1390–1396

2 Lin, Y., Wang, Y.-M.: 'Decision framework of group consensus with hesitant fuzzy linguistic preference relations', *CAAI Trans. Intell. Technol.*, 2020, **5**, (3), pp. 157–164

3 Smith, J.M., Price, G.R.: 'The logic of animal conflict', *Nature*, 1973, **246**, (5427), pp. 15–18

4 Li, S., Zhou, M., Luo, X., You, Z.-H.: 'Distributed winner-take-all in dynamic networks', *IEEE Trans. Autom. Control*, 2016, **62**, (2), pp. 577–589

5 Lippmann, R.: 'An introduction to computing with neural nets', *IEEE ASSP Mag.*, 1987, **4**, (2), pp. 4–22

6 Yang, J.-F., Chen, C.-M.: 'A dynamic K-winners-take-all neural network', *IEEE Trans. Syst., Man, Cybern., Syst.*, 1997, **27**, (3), pp. 523–526

7 Maass, W.: 'On the computational power of winner-take-all', *Neural comput.*, 2000, **12**, (11), pp. 2519–2535

8 Feng, R., Leung, C.-S., Sum, J.: 'Robustness analysis on dual neural network-based k WTA with input noise', *IEEE Trans. Neural Netw. Learn. Syst.*, 2017, **29**, (4), pp. 1082–1094

9 Jin, L., Li, S., La, H.-M., Zhang, X., Hu, B.: 'Dynamic task allocation in multi-robot coordination for moving target tracking: A distributed approach', *Automatica*, 2019, **100**, pp. 75–81

10 Zhao, X., Zong, Q., Tian, B., You, M.: 'Finite-time dynamic allocation and control in multiagent coordination for target tracking', *IEEE Trans. Cybern.*, In Press with DOI 10.1109/TCYB.2020.2998152

11 Qi, Y., Jin, L., Luo, X., Shi, Y., Liu, M.: 'Robust k-WTA network generation, analysis, and applications to multiagent coordination', *IEEE Trans. Cybern.*, In Press with DOI 10.1109/TCYB.2021.3079457

12 Wu, J., Xu, X.: 'Decentralised grid scheduling approach based on multi-agent reinforcement learning and gossip mechanism', *CAAI Trans. Intell. Technol.*, 2018, **3**, (1), pp. 8–17

13 McKee, D.W., Clement, S.J., Almutairi, J., Xu, J.: 'Survey of advances and challenges in intelligent autonomy for distributed cyber-physical systems', *CAAI Trans. Intell. Technol.*, 2018, **3**, (2), pp. 75–82

14 Cai, Z.-X., Ren, X.-P., Zou, L.: 'A simulated communications system for distributed multi-robots', *CAAI Trans. Intell. Technol. Syst.*, 2009, **4**

15 Lu, H., Jin, L., Zhang, J., Sun, Z., Li, S., Zhang, Z.: 'New joint-drift-free scheme aided with projected ZNN for motion generation of redundant robot manipulators perturbed by disturbances', *IEEE Trans. Syst., Man, Cybern., Syst.*, In Press with 10.1109/TSMC.2019.2956961

16 Liu, S., Wang, J.: 'A simplified dual neural network for quadratic programming with its KWTA application', *IEEE Trans. Neural Netw.*, 2006, **17**, (6), pp. 1500–1510

17 Zhang, X., Chen, L., Li, S., Stanimirović, P., Zhang, J., Jin, L.: 'Design and analysis of recurrent neural network models with non-linear activation functions for solving time-varying quadratic programming problems', *CAAI Trans. Intell. Technol.*, In Press with 10.1049/cit2.12019

18 Nazemi, A., Nazemi, M.: 'A gradient-based neural network method for solving strictly convex quadratic programming problems', *Cogn. Comput.*, 2014, **6**, (3), pp. 484–495

19 Liu, Y.-J., Tong, S., Chen, C.-P., Li, D.-J.: 'Adaptive NN control using integral barrier Lyapunov functionals for uncertain nonlinear block-triangular constraint systems', *IEEE Trans. Cybern.*, 2016, **47**, (11), pp. 3747–3757

20 Freeman, R.A., Yang, P., Lynch, K.M.: 'Stability and convergence properties of dynamic average consensus estimators', in *Proc. IEEE CDC*, San Diego, CA, USA, 2006, pp. 338–343

A Corresponding author

- Name: Long Jin;
- Gender: Male;
- Position: Professor;
- Institution: Lanzhou University;
- Postcode: 730000;
- Tel.: +86 18924236980;
- E-mail: longjin@ieee.org.